Biochemical and Computational Studies of Cadherin-23, a Protein Essential for Hearing

Undergraduate Research Thesis

Presented in Partial Fulfillment of the Requirements for graduation "with Honors Research Distinction" in the undergraduate colleges of The Ohio State University

by Florencia Velez-Cortes

The Ohio State University

December 2015

Project Advisor: Professor Marcos Sotomayor, Department of Chemistry and Biochemistry

Table of Contents

Figures Index

Tables Index

Statement of Research

I conducted the research presented in this thesis under the tutelage of Dr. Marcos Sotomayor of The Ohio State University Main Campus Chemistry and Biochemistry Department. I joined the Sotomayor lab in December of 2013, during my third year at the university. I have worked in his lab since with the exception of 10 weeks during the summer of 2014. I was trained in the process of protein purification and cell culture by visiting graduate student Deryanur Kilic in conjunction with Dr. Sotomayor. Dr. Sotomayor provided intellectual guidance in the design and performance of experiments, data analysis, and the writing of this thesis. The thermal melting experiments were performed in collaboration with Chemistry graduate student Deepanshu Choudhary. All simulations were performed at the Ohio Supercomputer Center with guidance and assistance from Dr. Yoshie Narui, Zach Johnson, and Dr. Raul Araya-Secchi. My research was generously funded by The Ohio State University Arts and Sciences Undergraduate Research Scholarship from summer 2014 until spring 2015. I performed research as a part of the Chemistry 4999H course as a requirement for the completion of an Honors Thesis.

This thesis is submitted to the College of Arts and Sciences at The Ohio State University in partial fulfillment of a degree with Honors Research Distinction.

Acknowledgments

I would like to thank Dr. Marcos Sotomayor for his indispensable help with the execution of this project and writing of this thesis. Not only has he provided the research guidance required to teach his students biochemistry laboratory and molecular dynamics techniques, but also creates a wonderful laboratory environment where collaboration and dialogue are encouraged. I am incredibly grateful to be a part of his research group. Postdocs Dr. Yoshie Narui and Dr. Raul Araya-Secchi fielded my numerous day-to-day questions concerning experimental and computational techniques, and I am very thankful for their patience. Yoshie has also been working alongside me every step of the way through the Drude equilibration and steered molecular dynamics. Zachary Johnson, a former undergraduate and now student at Marshall University Joan C. Edwards School of Medicine, worked out a lot of the bugs when he first began working with the Drude polarizable field, was very helpful in guiding me through VMD and NAMD, and will no doubt be an amazing doctor. Chemistry graduate student Deepanshu Choudary trained me to carry out the thermal assay. My initial training by visiting student Deryanur Kilic from Atatürk University introduced me to protein preparation techniques that were instrumental to this project. She also designed some of the constructs that I have been working with since she returned to Turkey. English B.A. graduate Cameron Bradford aided in organizing the references of this text, and provided meals and candid humor throughout the writing process. My family has cheered me on throughout my undergraduate career; their unconditional support drives my passion for research.

CHAPTER 1: INTRODUCTION

Hearing loss is the most common loss of perception in the world. Approximately 15% of people in the United States over 18 report some degree of hearing loss[1]. In addition, two to three out of every 1000 children in the United States are born deaf or hard-of-hearing[2]. As healthcare is improved across the United States and across the world, the population will become older and hearing loss more common. Deafness is related strongly to both environmental and genetic factors, which invites a variety of treatment approaches, including gene therapy[3] and local drug delivery[4].

This thesis focuses on cadherin-23, a non-classical cadherin that is crucial for auditory mechanotransduction[5–8]. I will first describe the function of cadherin-23 by providing an overview of the chemical and mechanical processes involved in hearing that take place in the inner ear, and I will summarize the research involving cadherin-23 up to date. In Chapter 2, I will describe the methods and results obtained in expressing cadherin-23 protein fragments in *E. coli* and purifying these constructs to produce protein amenable for use in X-ray crystallography. In Chapter 3, I will report my thermal melting experiments with deafness mutants of cadherin-23 to compare the stability of the mutants with that of wild type cadherin-23. Finally, I will detail the methods used in producing steered molecular dynamics simulations of cadherin-23 using the new polarizable Drude force field[9] and comparing these results to those obtained using the additive force field CHARMM36[10].

1. The Tip-Link in Sound Mechanotransduction

Hearing is a complex process that requires the perception and interpretation of mechanical waves as sound[11]. In mammals, sound waves are funneled into the inner ear through the ear canal, where they encounter the tympanic membrane. Sound waves cause reverberation of the tympanic membrane, which in turn causes the vibration of the ossicles, the hammer, anvil, and stapes. The reverb causes a pumping motion in the stapes, which is connected to the oval window of the cochlea (Fig 1). Pressure waves cause the motion of the perilymph inside the cochlea, which then causes the oscillation of the basilar membrane. Hair cells are responsible for sound mechanotransduction and are found between the tectorial and the basilar membrane, in the organ of Corti (Fig 2a). These hair cells possess a 'crown' of stereocilia arranged in a staircase-like manner (Fig 2b and 2c). When the basilar membrane is deflected upwards, it causes the hair cells' stereocilia to shear against the tectorial membrane, producing tension in the tip-link, a protein filament that opens ion channels to depolarize hair cells and begin the chain of mechanotransduction processes that lead to the sensation of sound[12–16] .

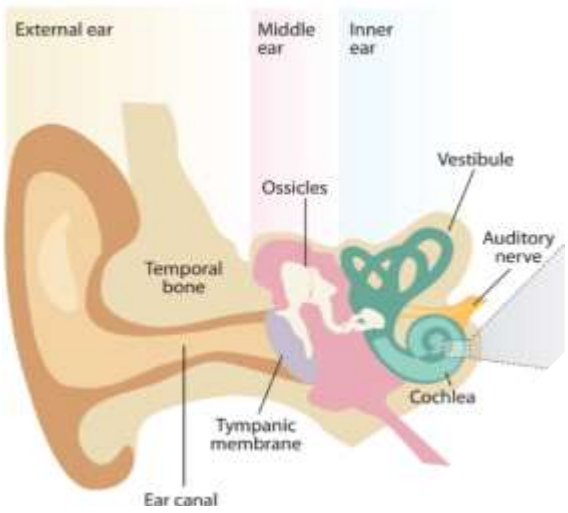

Figure 1. Schematic of the human ear. Adapted from [44]

The tip link is essential for inner—ear mechanotransduction and is made of two large cadherin proteins: cadherin-23 and protocadherin-15. These two proteins interact in an "extended handshake"[17] to form the tip-link, which connects the stereocilia of hair cells[13,18,19] (Fig 2c and

2d). It is expected that cadherin-23 and protocadherin-15 combine in a heterotetramer to form the tip-link[18].

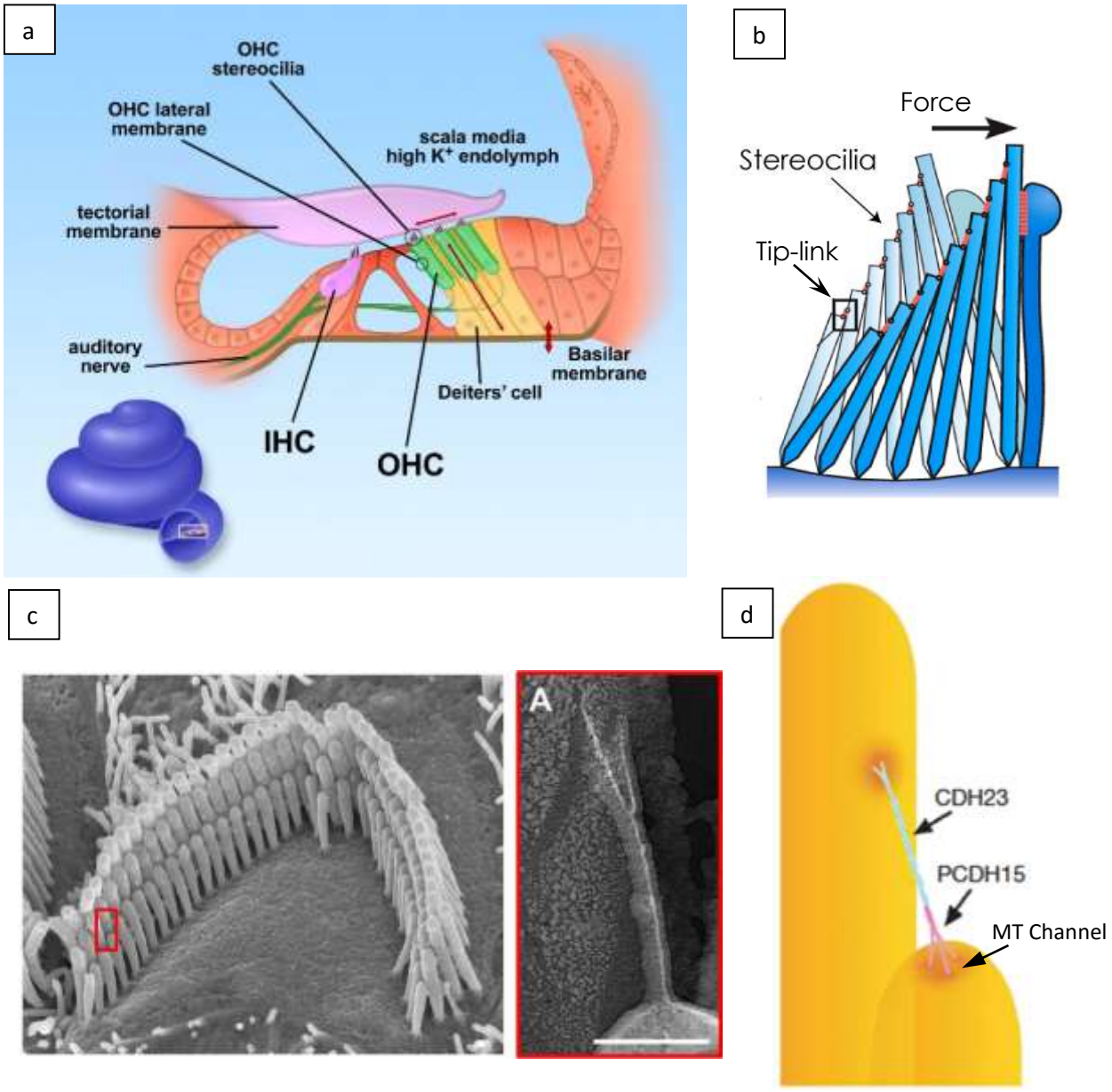

Figure 2. Hair cell mechanotransduction. a) Diagram of the organ of Corti, where sound mechanotransduction takes place [45]. b) Force produced by sound causes the deflection of stereocilia, tensing the tip-link which initiates the mechanotransduction of sound. Adapted from [17]. c) Electron micrographs of hair cells in guinea pig. Scale bar = 100 nm. Adapted from [19,46]. d) The tip link is made of cadherin-23 (CDH23) and protocadherin-15 (PCDH15). Adapted from[19,46]. Mechanotransduction (MT) channels are located at the base of the tip-link near PCDH15[15]. Adapted from [18].

2. The Cadherin Superfamily of Proteins and Cadherin-23

Multicellular organisms rely on cell adhesion to form the diversity of tissues and organs that comprise them. The bulk of this cell-to-cell connectivity is performed by the cadherin class of proteins; cadherins allow cells to communicate and physically bind to each other in a Ca^{2+}-dependent way. Cadherins are a superfamily of proteins involved in cell adhesion, development, and cancer[20]. They are fundamental for establishing and maintaining multicellular structures, particularly in vertebrate embryos[21]. Furthermore, cadherins have been shown to participate in intracellular signaling, with diverse roles in morphogenesis, sound transduction, and neuronal connectivity[22,23]. Although classical cadherins have been studied extensively, we know little about non-classical cadherins, such as cadherin-23.

Various members of the cadherin superfamily participate in homotypic or heterotypic interactions, i.e., they can connect with other identical molecules (homotypic) or with different members of the family (heterotypic). Classical cadherin proteins are typically comprised of a little over 700 amino acids and have a single transmembrane domain that divides the molecule into an amino-terminal extracellular and a carboxy-terminal cytoplasmic domain. The extracellular domain is made up of 5 repeating units called extracellular cadherin (EC) repeats, with well conserved motifs involved in Ca^{2+}-binding. Cadherin-23 is a non-classical cadherin and has 27 of such EC repeats, forming one of the largest members of the family in mammals (Fig 3a) with at least 26 of these Ca^{2+}-binding motifs. The structure of most of the cadherin-23 EC repeats are unknown. In chapter 2, I will describe our efforts to produce protein fragments for structural studies of cadherin-23.

3. Deafness Mutations in Cadherin-23

Cadherin-23 is a non-classical cadherin essential for hearing and has a large extracellular domain composed of 27 EC repeats in tandem, many of which are implicated in hereditary deafness[24–26] (Fig 3a and c). Genes that are mutated in Usher syndrome, the most frequent cause of deaf-blindness in humans, encode cadherin-23 among other proteins[27]. Missense mutations in cadherin-23 can cause deafness through a diversity of mechanisms (Fig 3c). Some missense mutations are located near or at Ca^{2+}-binding sites and may affect the protein's ability to bind Ca^{2+}. Other missense mutations are located at the binding interface with protocadherin-15 and may impair the formation of the tip-link. Others still can impair the protein's folding by disrupting its secondary structure. Interestingly, the cadherin-23 EC 13-15 fragment is the target of multiple single amino-acid mutations related to hereditary deafness[24,25,28]; five out of thirty-six in the entire extracellular portion of cadherin-23.

Two missense mutations in the cadherin-23 EC 13-15 fragment, an alanine to proline mutation at residue 1563 from the N-terminus of EC 1 (A1563P), and an arginine to glutamine mutation at residue 1484 (R1484Q), are not near Ca^{2+}-binding sites. Mapping of these mutations to the structure of cadherin-23 EC 1-2 confirms their location within the EC repeats, but far from Ca^{2+}-binding sites. These mutations could affect parallel dimerization of cadherin-23 or impair protein stability. In Chapter 3, I discuss how I determined the melting temperature of the wild-type and mutant cadherin-23 EC 13-15 fragments.

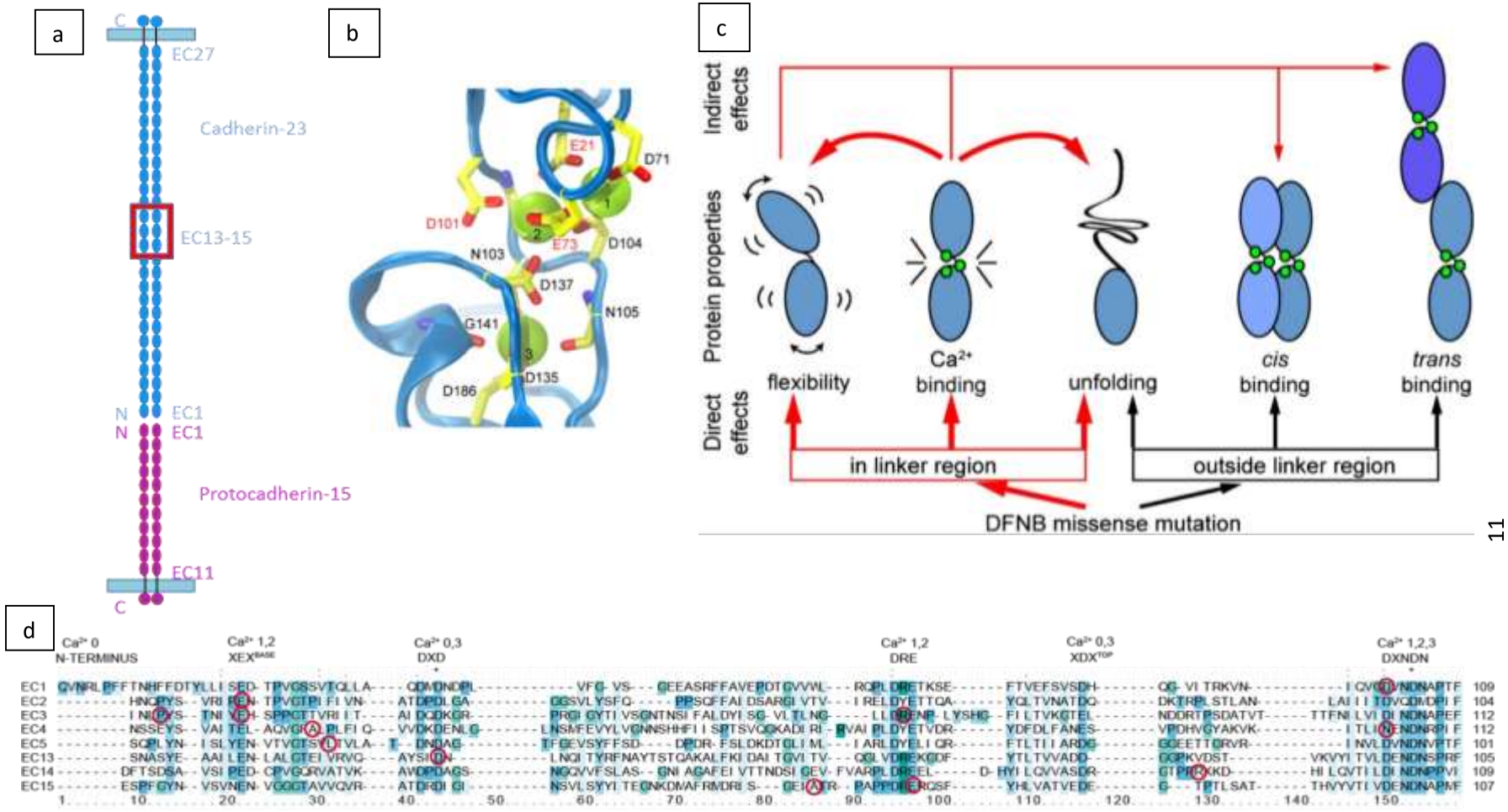

Figure 3. Tip-link and cadherin-23. a) The tip-link is composed of cadherin-23 and protocadherin-15, which are made of "repeating" units called EC repeats. The fragment of interest for crystallization and thermal melting is EC 13-15 (red box). b) Detail of Ca^{2+}-binding site in cadherin-23 EC 1-2. c) Possible effects of EC repeat missense mutations depend on the location of the mutation. Adapted from [29]. d) Alignment of cadherin-23 EC repeats of interest for this thesis. Mutations linked to deafness are circled in red. Amino acid motifs forming Ca^{2+}-binding sites are shown above alignment (XEX^{BASE}, DXD, DRE, XDX^{TOP}, DXNDN). Adapted from [29].

4. Importance of Ca^{2+} for the Integrity of Cadherin-23

Ca^{2+} is essential for the function of cadherins and in particular, for the function of cadherin-23 in inner ear mechanotransduction. When Ca^{2+} is removed from the extracellular medium that bathes the tip-link using a chelator (BAPTA), mechanotransduction currents disappear along with tip-links[14]. In addition, multiple missense mutations are predicted near or at Ca^{2+}-binding sites of cadherin-23. Previous simulations studies have shown that Ca^{2+} is essential for the mechanical strength of cadherin-23[29]. In these simulations an external force is applied to mimic the physiological stimulus experienced by the tip-link. In addition, low Ca^{2+} concentration conditions, such as in the cochlear endolymph which surrounds the tip-links (20-40 μM) [30,31], were modeled in simulation by removing Ca^{2+} from the binding sites of cadherin-23. These simulations showed that in the presence of Ca^{2+}, the protein is mechanically strong and unfolding forces are large, while in the absence of Ca^{2+} the force required to unfold EC repeats is reduced.

Protein simulations of cadherins have been performed using additive force fields such as CHARMM36, which uses point charges centered on atoms. Recently, a polarizable field has been developed which introduces an auxiliary charged particle attached to the nucleus via a harmonic spring to effectively capture the charge redistribution in response to changes in local electric fields[9]. This so-called "classical Drude oscillator force field" has been shown to accurately represent interactions between ions and proteins[32], yet the appropriate parameters to perform steered molecular dynamics simulations using this improved force field are unknown. I performed equilibration simulations and pullings of the previously crystallized cadherin-23 EC 1-2 structure[17], and compared the temperature stability of cadherin-23 simulations for different parameter values, as described in Chapter 4.

CHAPTER 2: EXPRESSION AND PURIFICATION OF CADHERIN-23 FRAGMENTS

Through evolution, organisms optimize the structure of proteins to fit functional demands. Although the involvement of cadherin-23 in hearing is crucial (Section 1.3), it is unclear whether the role of cadherin-23 is that of a stiff cable, or whether cadherin-23 is the gating spring that modulates the mechanical gating of the hair cell channels[33]. Elucidating the structures of cadherin-23 fragments could allow us to measure the elasticity of cadherin-23 and thus, computationally, help interpret single molecule experiments testing its mechanics. This should determine the role of cadherin-23 in hearing mechanotransduction. To this end, I designed fragments of cadherin-23 for cloning, expression, and purification to produce protein amenable for crystallization. In addition, I designed a refolding assay based on [34] to aid in the refolding of protein fragments that would not respond well to large-scale refolding protocols currently used for cadherins.

1. Methods: Cloning of Cadherin-23 Fragments

Due to the size of cadherin-23, smaller fragments constituting 2 to 3 consecutive EC repeats were designed using cDNA of *Mus musculus* and *Homo sapiens* sources. The *E. coli* expression system was used to express the milligram quantities of protein required for large-scale protein preparations employed in common structural studies involving nuclear magnetic resonance (NMR) and X-ray crystallography.

Homo sapiens Cadherin-23 was ordered as a synthetic gene from Bio Basic Inc. and *Mus musculus* cadherin-23 was obtained from U. Mueller at the Scripps Research Institute through Dr. David Corey at Harvard Medical School. The fragment constructs were designed by using the published structure of cadherin-23 EC 1 and 2 (Protein Data Bank code 4APX[17]) as a

reference in conjunction with sequence alignments of cadherin-23 EC repeats to avoid disrupting predicted secondary structure features. The desired fragments were obtained through PCR amplification. To this end, I designed primers that could anneal themselves to either end of the desired fragment in the parental DNA strand. These primers included a short spacer sequence (5'-CCGCCG-3') and the sequence of NdeI and XhoI enzyme restriction sites (5'-CATATG-3' and 5'-CTCGAG-3', respectively) in tandem with the complementary sequence to the region of the gene to be cloned.

The amplified sequence was then digested with restriction enzymes NdeI and XhoI, and ligated to a similarly digested pET21a(+) plasmid vector. The pET21 vector carries an ampicillin resistance gene, an isopropyl β-D thiogalactopyranoside (IPTG) inducible T7 promoter, and a C-terminal six-histidine tag to allow for the Ni-affinity purification of the expressed gene fragment. I propagated DNA plasmids using the DH5α *E. coli* strain. The insertion of cadherin-23 gene fragments was verified by NdeI and XhoI enzyme digestions and agarose gel analysis to observe the approximate length of the insert. Additionally, the gene fragment sequence was verified by sequencing with the T7 promoter and T7-terminator primers.

2. Methods: Protein Expression

The expression of cadherin-23 constructs was performed either in BL21-Gold (DE3) or BL21-CodonPlus (RIPL) *E. coli* cells. The latter were used for constructs of cadherin-23 fragments that coded for multiple rare codons. Both strains of *E. coli* contain the T7 polymerase gene to allow for the induction of protein expression through the addition of IPTG to the growth medium. These strains have been modified for high protein production. All BL21 cells were grown in Lysogeny Broth (LB) medium.

Overnight cultures were inoculated with single colonies of transformed BL21 cells and allowed to grow overnight. Then, a small-scale 25-mL expression culture with 100 µg/mL of ampicillin was inoculated with 200 µl of the overnight culture and incubated at 37°C until the culture reached an OD_{600} of 0.4, at which point IPTG was added for a final concentration of 200 µM. The cells were grown at 30°C overnight, and then were pelleted. The pellets were resuspended in SDS-gel loading buffer and boiled. The sample was then loaded onto a SDS-PAGE gel and stained with Coomassie to determine whether the protein fragment of interest was expressed. The protein was then expressed at a large scale for use in biochemical assays and crystallization testing. For this purpose, a 2-L culture was inoculated with 25 mL of overnight BL21 cell culture. The cells were grown at 37°C until the culture reached an OD_{600} of 0.4. The culture was then induced with IPTG (200 µM final concentration) and incubated overnight at 30°C. On the following day, the culture was pelleted and stored at -20°C.

3. Methods: Purification and Refolding

Cadherin-23 fragments tend to form inclusion bodies, or aggregates, inside the cytoplasm of *E. coli*[29]. For this reason, cadherin-23 fragments were purified under denaturing conditions. The pelleted cells were lysed by sonication in denaturing binding buffer (20 mM Tris-HCl pH 7.5, 10 mM $CaCl_2$, 6 M guanidinium hydrochloride, and 20 mM imidazole pH 7.5). Approximately 50 mL of binding buffer was added to 8 g of cell pellet. The lysate was then centrifuged at 20,000 rpm for 30 minutes at 4°C to remove cellular debris. The protein-rich supernatant was incubated with Ni-sepharose high performance resin for one hour at 4°C. After incubation, I centrifuged the mixture at 3,000 rpm for 5 minutes at 4°C and discarded the supernatant. After washing the nickel beads with binding buffer, I centrifuged the mixture and displaced the protein from the resin using a denaturing elution buffer with high imidazole concentration (20 mM Tris-HCl pH

7.5, 10 mM $CaCl_2$, 6 M guanidinium hydrochloride, and 500 mM imidazole pH 7.0). The protein elution was diluted to <0.5 mg/mL and then dialyzed at 4°C overnight against a non-denaturing dialysis buffer (20 mM Tris-HCl pH 8.0, 5 mM $CaCl_2$, 150 mM KCl, 50 mM NaCl, 400 mM Arginine), which removes guanidinium hydrochloride from the protein solution to promote refolding of the protein fragment. The dialyzed protein was collected and centrifuged at 20,000 rpm for 30 minutes at 4°C to possible amounts of precipitation. Then, the supernatant was concentrated with a 10,000 MWCO polyethersulfone (PES) membrane to the desired volume for use in size-exclusion chromatography, with a protein concentration ranging between 2 and 10 mg/mL for preparative purposes and much lower for analytical chromatography.

To isolate refolded protein I used size exclusion chromatography. This method employs a porous resin column that traps proteins with low hydrofluidic volume while higher volume protein bypasses the maze-like pores and is then eluted earlier from the column (Fig 4).

A S200 Superdex 16/60 GL (GE Healthcare) was used to purify large-scale protein preparations after equilibrating the column in 20 mM Tris HCl (pH 8.0), 50 mM NaCl, 150 mM KCl, and 5 mM $CaCl_2$. The concentrated protein was filtered prior to loading onto the column using a 0.45 µm PES membrane. The purity and integrity of the protein in the eluted fractions was assessed using Coomassie-stained SDS page. A S200 3.2/30 GL (GE Healthcare) column was used to purify small-scale protein for analytical purposes, which was equilibrated with the same buffer as above.

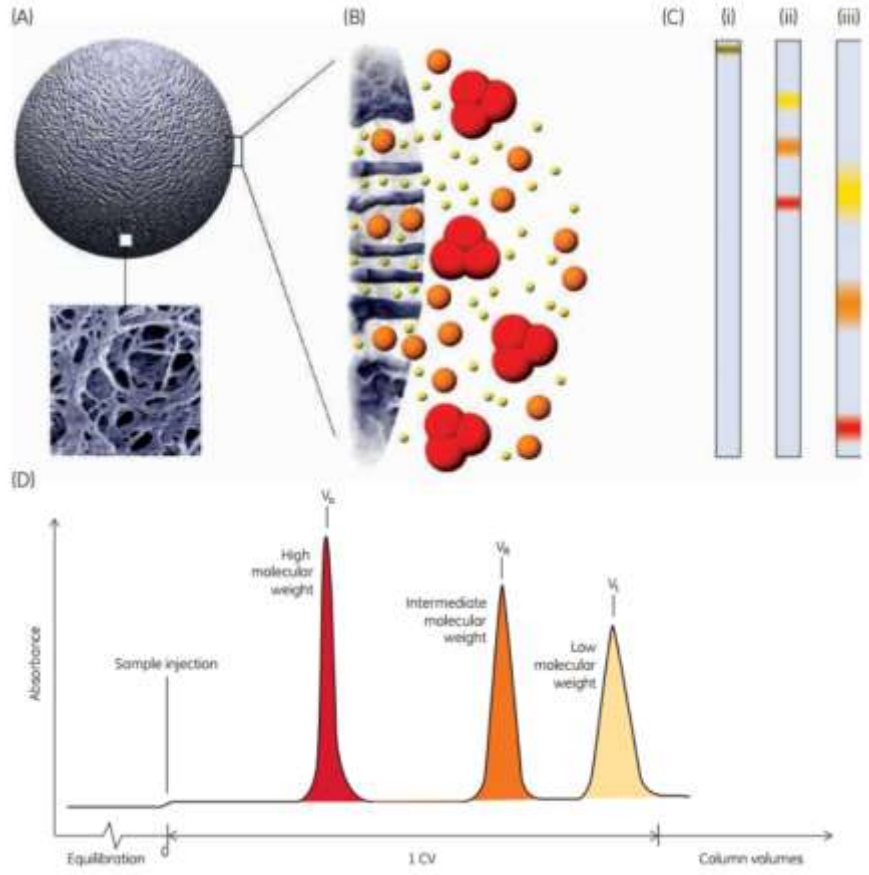

Figure 4. Size exclusion chromatography. A) Illustration of a resin bead B) interacting with molecules of various hydrofluidic volume. C) Size-exclusion chromatography separates samples of differing molecular weight and D) elutes each molecular size at a different elution volume. Adapted from [47].

4. Methods: Refolding Screen

To test and find efficient refolding conditions for protein fragments that did not refold well using the dialysis protocol described above, a refolding screen was prepared based on [34] with modifications by Dr. Wilhelm A. Weihofen. 96 refolding buffers were prepared as shown in Figure 5a. Protein purified in guanidinium hydrochloride was concentrated to 4 mg/mL using a 10,000 MWCO PES membrane concentrator. 10 µl of concentrated protein were aliquoted into each well of a 96-well non-binding plate. Over the course of 18 hours, the protein was diluted

with refolding buffer as indicated in Figure 5b. Conditions were pre-screened for aggregate by measuring absorbance at 320 nm wavelength.

5. Methods: Protein Crystallization

Thus far, we have produced refolded, purified protein which can be used for X-ray crystallography. We have begun attempting crystallization of these constructs using the hanging drop method with buffers from QIAGEN protein crystallization screens.

Human cadherin-23 EC 13-15 fractions were concentrated to 10 mg/mL and aliquoted into a 96-well plate with a sitting drop reservoir. 75 µl of buffer from QIAGEN protein crystallization screens were aliquoted into the large reservoir, with a v/v ratio of 0.6 µl protein solution to 0.6 µl crystallization buffer, and also with ratios of 1 µl protein solution to 0.5 µl buffer, and vice versa. The buffer in the protein well evaporates until the concentration of buffer in the two wells equalizes. These trays are checked periodically for crystals.

6. Results: Cloning, Protein Expression and Purification, and Crystallography

Table 1 summarizes the progress of each construct I have produced since I joined Dr. Sotomayor's laboratory, some of which were prepared using Deryanur Kilic's primers (designated DK in the table). Human cadherin-23 EC 13-15 (short, DK) and mutant variants A1563P and R1484Q refolded successfully with standard dialysis, as shown by size-exclusion chromatography (Figure 6). SDS –PAGE analysis of representative elution fractions were performed and showed the desired fragment was present.

a

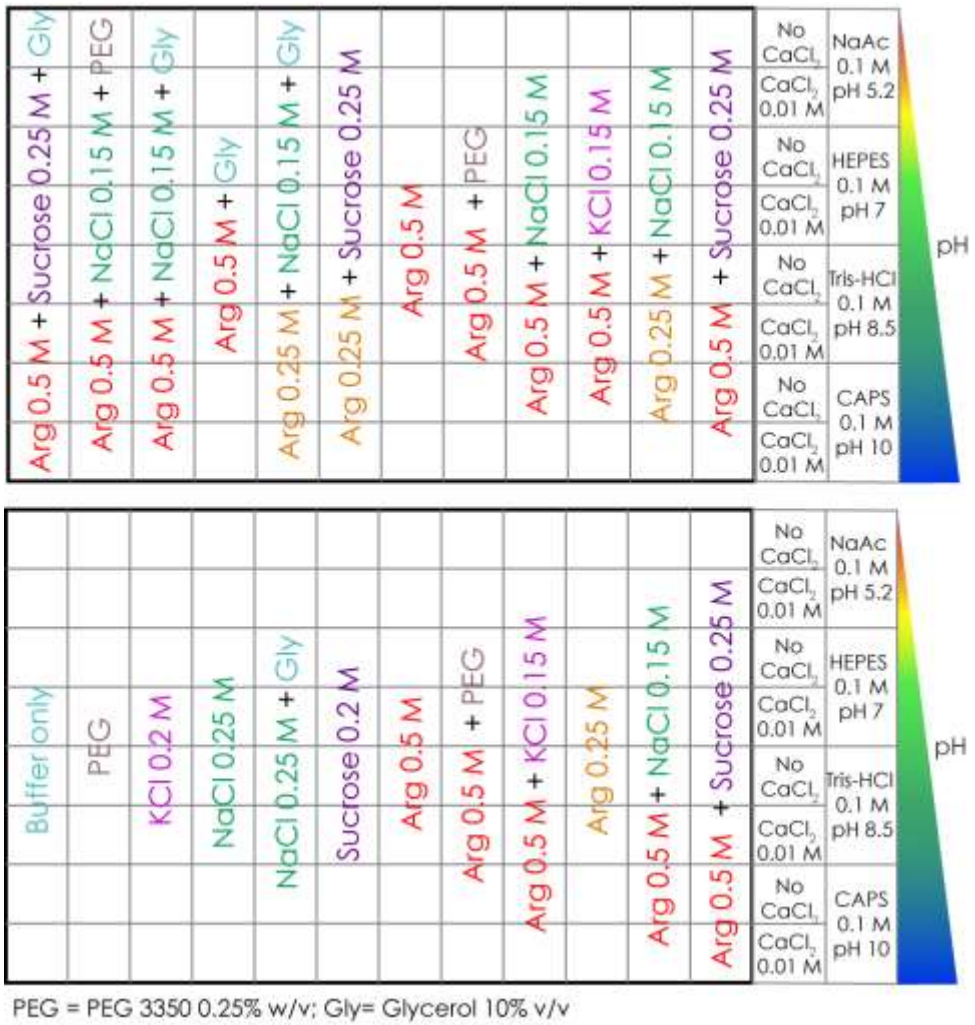

PEG = PEG 3350 0.25% w/v; Gly= Glycerol 10% v/v

b

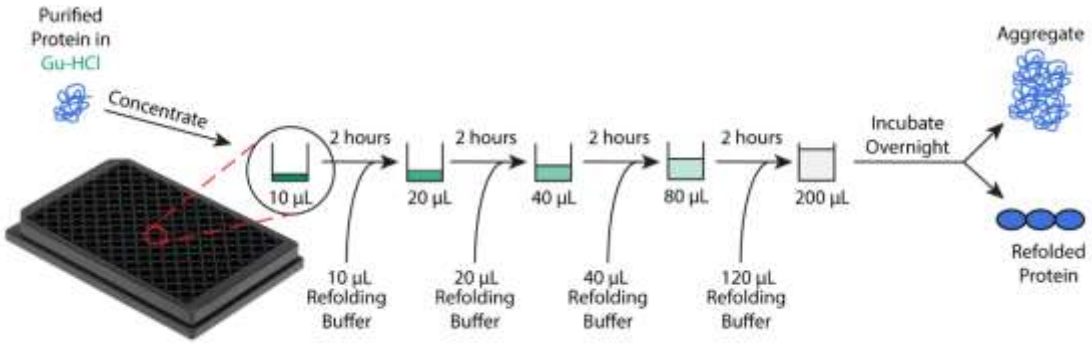

Figure 5. Refolding screen for cadherins. a) Refolding screen buffers designed based on [34]. b) Protein purified under denaturing conditions can be refolded after a series of dilutions with refolding screen buffers.

Construct	Primers	DNA	Exp	Ref	SEC	Conc	Crystal	Diff	Structure
hs3-4	•	•	•	x					
hs3-5	•	•	•	x					
mm3-4	•	•	•	x					
mm3-5	•	•	•	x					
hs11-14	•	~							
hs11-15	•	•	~	x					
mm12-16	•	•	~						
hs13-15 (short, DK)	•	•	•	•	•	•	x		
hs13-15 (long, FV)	•	•	•	•	•	•	x		
hs13-15Q1473H (DK)	•	•	•	•	•	•	?		
hs13-15R1484Q (DK)	•	•	•	•	•				
hs13-15A1563P (DK)	•	•	•	•	•				
mm13-14	•	x							
mm13-15	•	•	•	•	•	•			
mm13-16	•								
hs14-16	•	•	•	x					
mm14-16	•								
mm14-15	•	x							
hs14-15	•								
mm15-16	•	•							

Table 1. Cadherin-23 fragments I have designed during my work in Dr. Sotomayor's laboratory. Each major step towards obtaining the structure of a protein via X-ray crystallography is listed in the first row.

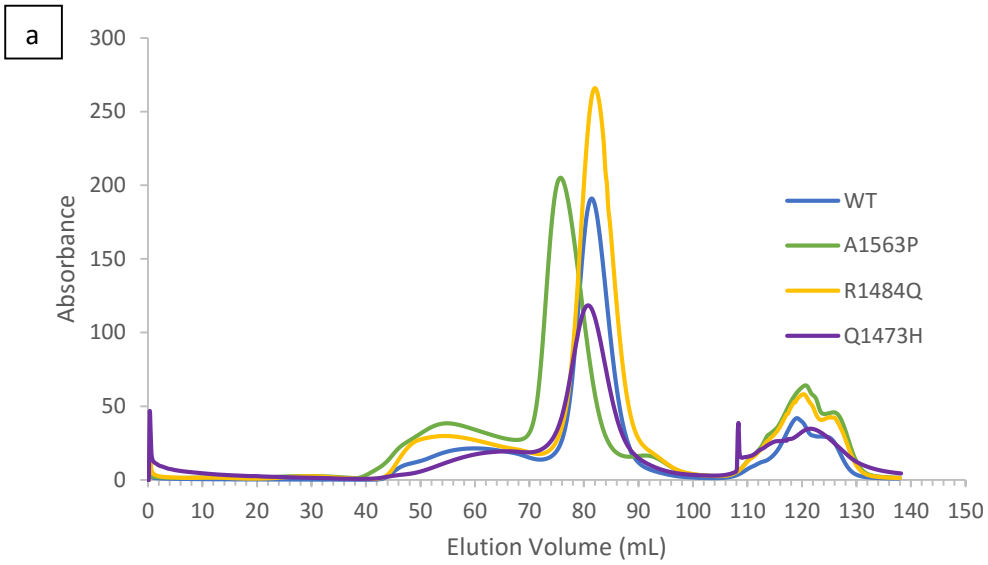

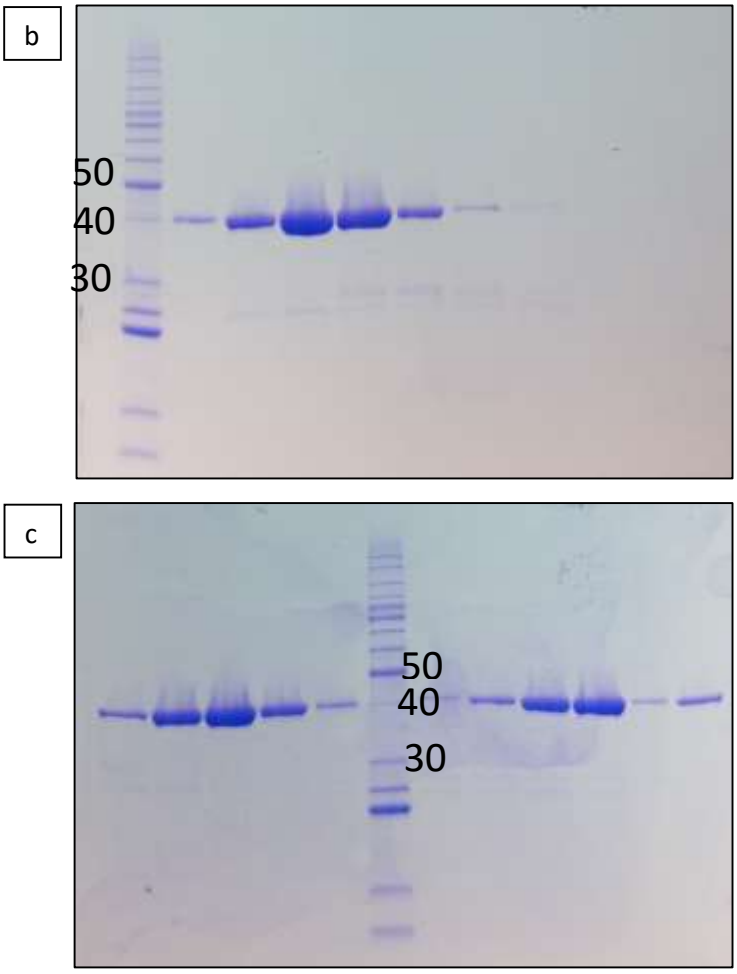

Figure 6. Size-exclusion chromatography (S200 16/600) of large-scale protein preparations. a) Size-exclusion chromatography of human cadherin-23 EC 13-15 wild-type (WT) and variants (A1563P, R1484Q, Q1473H). b) Example of SDS-PAGE showing the desired protein (cadherin-23 EC 13-15 R1484Q). c) SDS-PAGE gel showing peak fractions for cadherin-23 EC 13-15 A1563P (left of ladder) and cadherin-23 EC 13-15 wild-type (right of ladder). The predicted molecular weight of the wild-type cadherin-23 EC 13-15 fragment is 35 kDa.

7. Results: Refolding Screen

When standard protein refolding (as mentioned in section 4) was unsuccessful, we used a refolding screen. This method was attempted for cadherin-23 constructs of EC 3-4 and EC 3-5, which are next to repeats EC 1 and EC 2 that refold well and for which there are structures. None of the tested conditions efficiently refolded my constructs. Human cadherin-23 EC 3-5 was not successfully refolded using the protocol detailed in Section 2.3 (Figure 7). However, this refolding screen proved successful for the refolding of Dr. Narui's construct as shown by analytical size-exclusion chromatography (Fig 8).

8. Conclusions

Determination of the structure of cadherin-23 fragments could help elucidate the role of cadherin-23 in hearing mechanotransduction. To this aim, I have produced folded cadherin-23 protein fragments of EC 13 through 15 and three of its mutant variants, Q1474H, R1484Q, and A1563P. I have also designed a refolding screen which can aid in streamlining the refolding process of other cadherin-23 fragments. The constructs of cadherin-23 EC 13-15 wild-type and mutant variants A1563P and R1484Q will also be used in thermal melting assays to determine the difference in stability of their secondary structures.

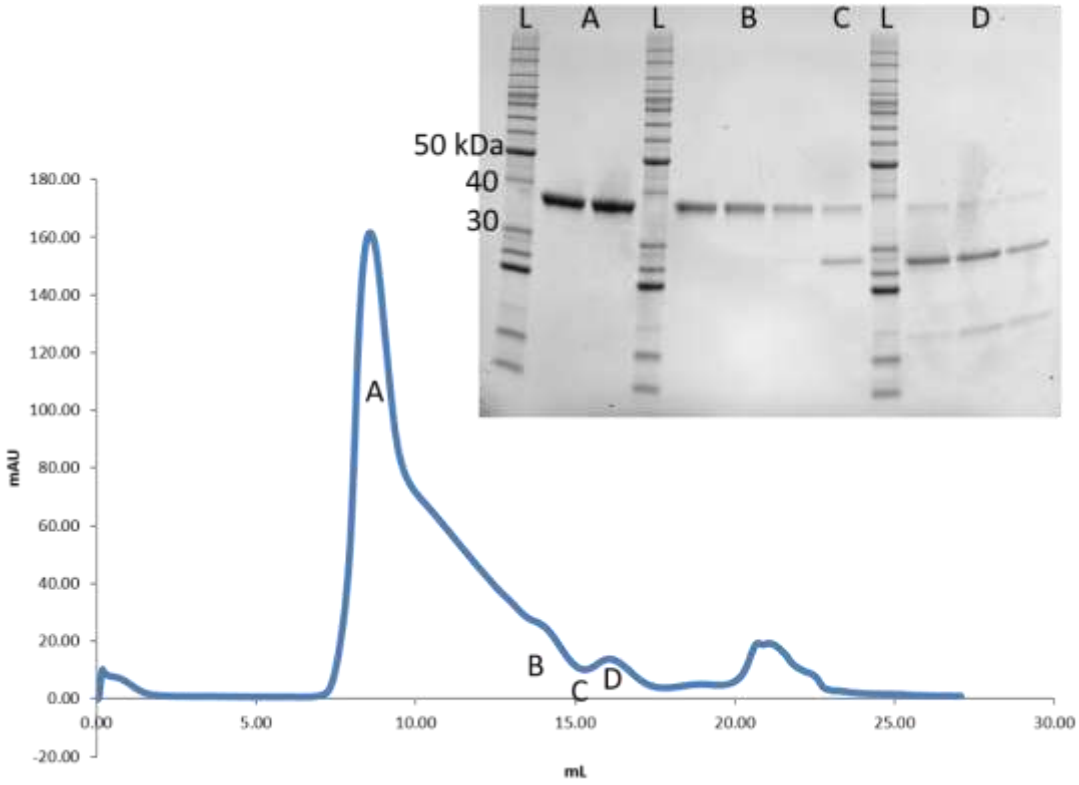

Figure 7. Size exclusion chromatography (S200 10/300) of human cadherin-23 EC 3-5 (36 kDa), which degraded, aggregated or precipitated in most buffer solutions. Refolded protein of 36 kDa elutes at ~13.5 mL in this column.

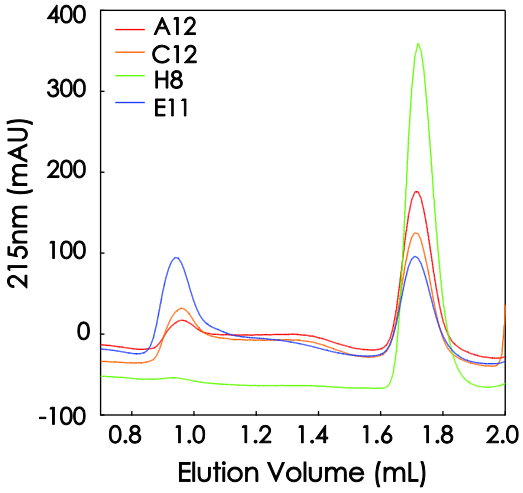

Figure 8. Size-exclusion chromatography (S200 3.2/30 GL) of ancestral cadherin-23 protein refolded with refolding assay. Refolded protein elutes at ~1.7 mL and aggregated protein elutes at ~1 mL. Refolding screen identified a condition (H8) in which no aggregate was observed. Data and figure courtesy of Dr. Yoshie Narui.

CHAPTER 3: THERMAL MELTING OF CADHERIN-23 MUTANTS

Multiple mutations linked to deafness modify the extracellular domain of cadherin-23[24–26,35]. Although many of these mutations are found at or near Ca^{2+}-binding sites, some of the mutations do not appear to be involved in the binding of Ca^{2+} by cadherin-23. Among these mutations are variants A1563P and R1484Q, which are named by the amino acid found in wild-type cadherin-23, followed by the amino acid number and the amino acid it has been changed to. In A1563P, an alanine (small, hydrophobic side chain) is mutated to a proline (bulky cyclic side chain), while in R1484Q, an electrically charged arginine side chain is replaced by a polar uncharged side chain. These mutations could disrupt the secondary structure of the extracellular cadherin repeat by introducing steric hindrance. Alternatively, the mutation from alanine to proline could disrupt the formation of an alpha helix or beta strand due to its tendency to disrupt backbone hydrogen bonds.

Using the alignment in Fig 3d as a guide, I matched cadherin-23 mutation sites A1563P and R1484Q to their counterparts in EC 1 and 2 of cadherin-23 wild-type, of which there is already a structure. I mapped mutations A1563P to residues I92 and P193 in EC 1 and EC 2 of cadherin-23, respectively. The placement of this residue with respect to the beta strands in EC 1 suggested that this mutation may be responsible for disrupting protein stability (Fig 9a), while the EC 2 counterpart was much closer to a Ca^{2+}-binding site, which may be the target of this mutation (Fig 9b). Mutation R1484Q mapped to W66 in EC 1, which is not near a Ca^{2+}-binding site, and thus the mutation is likely reducing the stability of the protein (Fig 9c).

Thermal melting can determine the stability of the secondary structure of a protein. Upon thermally-induced melting we can observe a sharp transition between the folded and unfolded

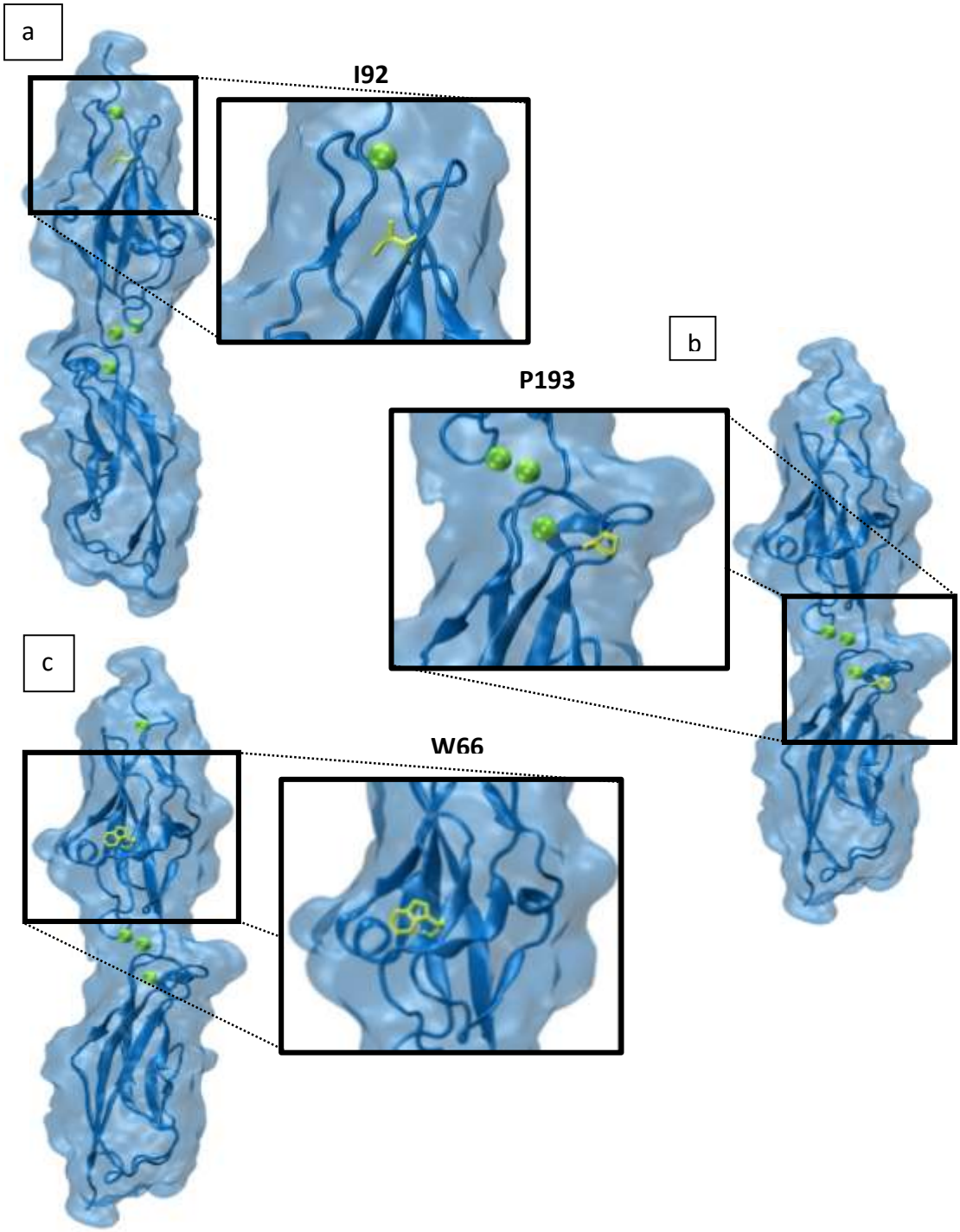

Figure 9. Mapping of A1563P suggests that the mutation could be affecting a) folding of the protein or b) the ability of cadherin-23 to bind Ca^{2+}. c) Mapping of R1484Q shows that a mutation at this site could disrupt secondary structure features.

states, where the melting temperature (T_m) is defined as the midpoint of the protein unfolding transition[36]. In this chapter I will compare the results obtained for thermal melting experiments of cadherin-23 EC 13-15 wild-type and deafness-related mutants A1563P and R1484Q.

1. Methods: Mutagenesis of Wild-Type Cadherin-23

To generate cadherin-23 variants A1563P and R1484Q, I used the site-directed mutagenesis QuikChange Lightning kit by Agilent. The mutagenesis primers were made using the Agilent primer design tool. The primers are composed of the complementary sequence encoding the missense mutation of interest such that when the primers are used in PCR with the parental wild-type cadherin-23 sequence, the PCR product contains the codon coding for proline in place of alanine (in the case of the A1563P variant) and glutamine in lieu of arginine (for the R1484Q variant). The parental strand was degraded using the Dpn I enzyme, which targets methylated DNA. The product of the enzyme digestion was used to transform DH5α *E. coli* cells. The cells were lysed and the new vector was purified using the QIAGEN Miniprep kit and sent for sequencing. Protein expression-specialized BL21 Codon Plus cells were transformed with the miniprepped and sequenced vectors. Expression and purification were performed as explained in Chapter 2.

2. Methods: High-Throughput Thermal Screening

Refolded wild-type, A1563P, and R1484Q *H. sapiens* cadherin-23 EC 13-15 protein were produced and purified by size-exclusion chromatography (Chapter 2) and diluted to 0.3 mg/mL. Sypro® Orange protein stain was added to each protein solution and the mixture was aliquoted

into a 96-well plate. A real-time PCR machine was used to gradually heat the sample from 10°C to 95°C for 425 cycles, increasing the temperature by 0.2 °C each cycle. Simultaneously, fluorescence changes were measured for wavelength of emission at 575 nm. The Sypro® Orange dye binds non-specifically to the hydrophobic portions of proteins, which are hidden when these are folded in an aqueous solution. As the temperature increases, proteins unfold and the dye fluoresces as it binds to exposed hydrophobic patches (Figure 10).

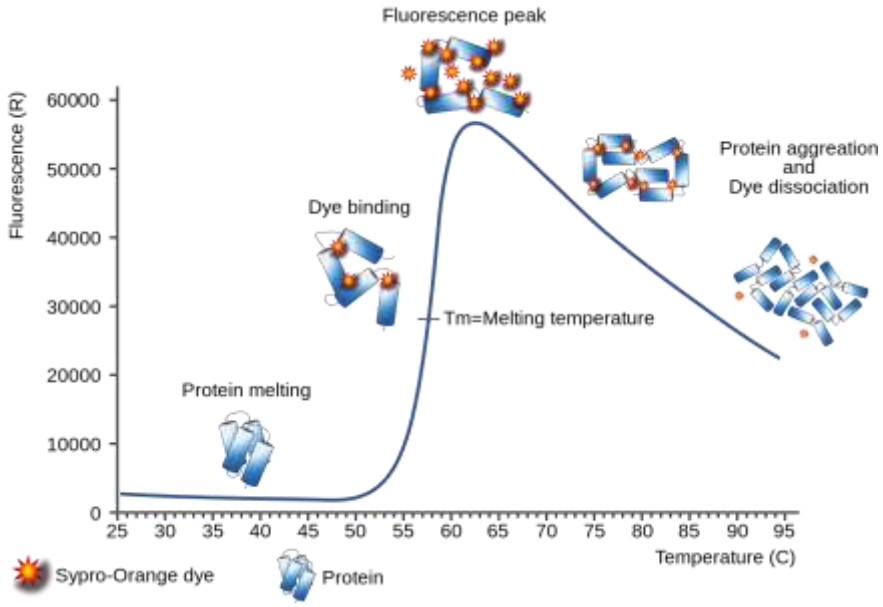

Figure 10. Sypro-orange dye binds non-specifically to hydrophobic portions of protein which only become exposed in aqueous solution if the protein is not folded. The dye fluoresces upon binding. Courtesy of Goran Tek-en via Wikimedia Commons.

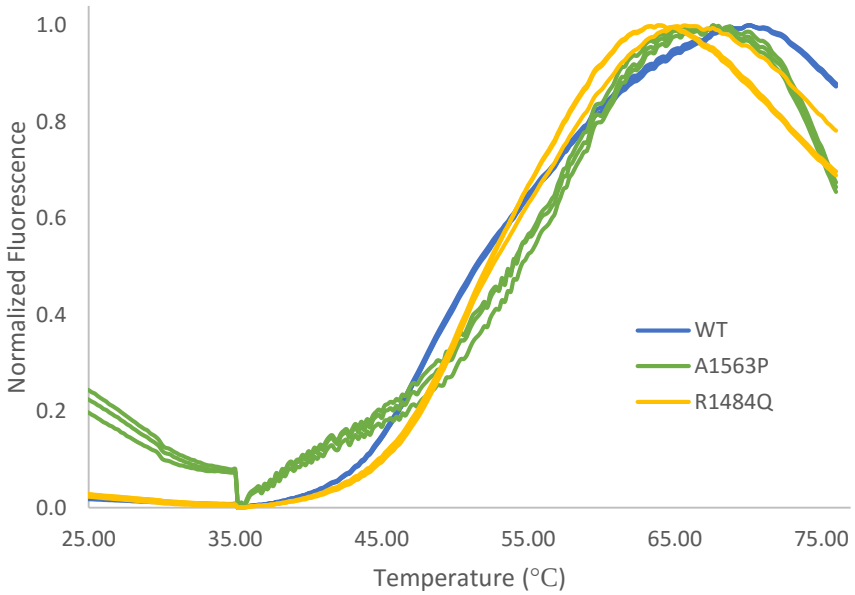

Figure 11. Normalized thermal melting curves for human cadherin-23 wild-type and deafness-related mutants.

3. Results: Melting Temperatures of Wild-type and Mutant Cadherin-23

Each cadherin-23 EC 13-15 variant thermal screening was performed in triplicate. The fluorescence signal was normalized to the maximum intensity of the three variants, excluding data points after the fluorescence intensity maximum. Figure 11 shows the normalized fluorescence measured by real-time PCR.

The melting temperature for each variant was calculated by finding the temperature at which the normalized fluorescence reached 0.5, and a summary of the results is in Table 2 and Figure 12. The melting temperatures of mutants A1563P and R1484Q were similar to that of wild-type cadherin-23, suggesting that the secondary structure of the mutant variants is not significantly altered.

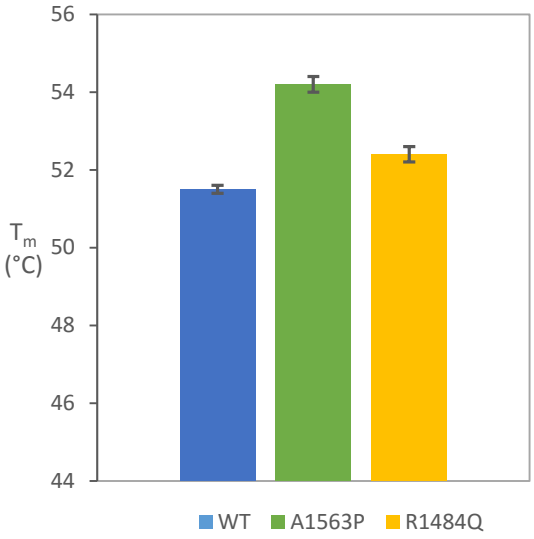

Figure 12. Melting temperature differences for all variants.

	WT	A1563P	R1484Q
Melting Temperature (°C)	51.5 ± 0.1	54.2±0.2	52.4±0.2

Table 2. Melting temperatures of human cadherin-23 variants. Standard deviations from triplicates are shown.

Although the melting temperatures of mutant and wild-type variants of cadherin-23 EC 13-15 were similar, the quality of the melting curves is poor, and could be unreliable. In particular, the A1563P variant shows discontinuities in fluorescence and displays non-zero fluorescence prior to the unfolding transition peak.

4. Conclusions

Thermal melting of cadherin-23 EC 13-15 fragment of wild-type and A1563P and R1484Q variants was not found to be significantly different. However, these experiments were performed after one week of purifying the protein fragments by size-exclusion chromatography. Repetition of these experiments with an additional size-exclusion chromatography purification step or a smaller time frame between chromatography and the performance of high-throughput thermal screening (in order to avoid aggregation of unstable protein) may improve the quality of the melting curves and allow a statistical analysis of the small differences observed.

CHAPTER 4: MOLECULAR DYNAMICS SIMULATIONS OF CADHERIN-23

The gating of hair cell channels is modulated by a gating spring, which could be formed by the tip-link. Mechanical measurements of hair bundles indicate that this gating spring element has a stiffness of 1 mN/m[33,37] . SMD simulations of cadherin-23 EC 1 and 2 found that the overall elasticity of these repeats was 570 mN/m, which, even when extrapolated to 38 EC repeats, is too stiff to be the gating spring. However, their elasticity is highly dependent on the ions bound to its linker regions[29], and these simulations were performed using the CHARMM27 force field, which is limited in its description of divalent ion-protein interactions[38,39]. A new polarizable force field has been developed in which part of the atomic charge is modeled as an extra particle which is attached to the nucleus and oscillates harmonically around it[9] (Fig 13). This new method and force field, called the Drude polarizable force field, has yielded results in molecular dynamics simulations that are comparable to empirical methods[32]. Because simulations can give important insights on the stiffness of cadherin-23, its potential as a gating spring candidate, and the effect of mutations on its strength and stability, it is worth revisiting cadherin-23 simulations with the improved Drude modelling of polarization effects by Ca^{2+}. Our aim is to create a protocol with appropriate parameters for the equilibration of cadherin-23 using the Drude force field. We also produced a protocol to carry out steered molecular dynamics simulations with the

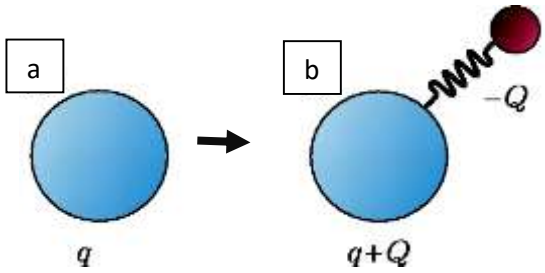

Figure 13. The Drude polarizable force field adds a practically massless charged (-Q) particle to each atom (originally charged q). Adapted from[48].

Drude force field and compare our results with the previous CHARMM27 pullings of cadherin-23. Our simulations are performed using the NAMD molecular dynamics engine[40,41] and analyzed with VMD. This project was performed with Dr. Yoshie Narui and Zachary Johnson.

1. Simulation Setup: Configuration Files

To test the elasticity of cadherin-23 EC 1-2 using the Drude polarizable force field, I used the CHARMM-GUI Drude Prepper to introduce Drude particles to our simulation system. I tested several Langevin values for Cadherin-23 EC 1-2 SMD simulations following equilibration of our system using the output from the CHARMM-GUI Drude Prepper.

The CHARMM-GUI Drude Prepper[42], generates NAMD configuration files that use the Langevin thermostat to control temperature. The Langevin equation used in this model includes a damping constant γ that controls the coupling of the thermostat to the system. Large values of γ result in tight temperature control, but introduces artificial dampening of atomic motions. Small values of γ are preferred, especially for steered molecular dynamics (SMD) simulations in which atoms and proteins move at fast speeds and may experience artificial frictional forces from the thermostat. Unfortunately, the CHARMM-GUI Drude Prepper generates configuration files with large values for the damping coefficients controlling the general dynamics of atoms (γ_G –general Langevin damping) and the dynamics of Drude particles (γ_D – Drude Langevin damping). These parameters are unsuitable for our SMD simulations, so I tested several different Langevin values for γ_D and γ_G using the cadherin-23 EC 1 and 2 system as a model (Fig 14). The PSF and PDB files produced by the Drude Prepper Input Generator included coordinates and velocities for 161,399 atoms, of which 64,688 were Drude particles.

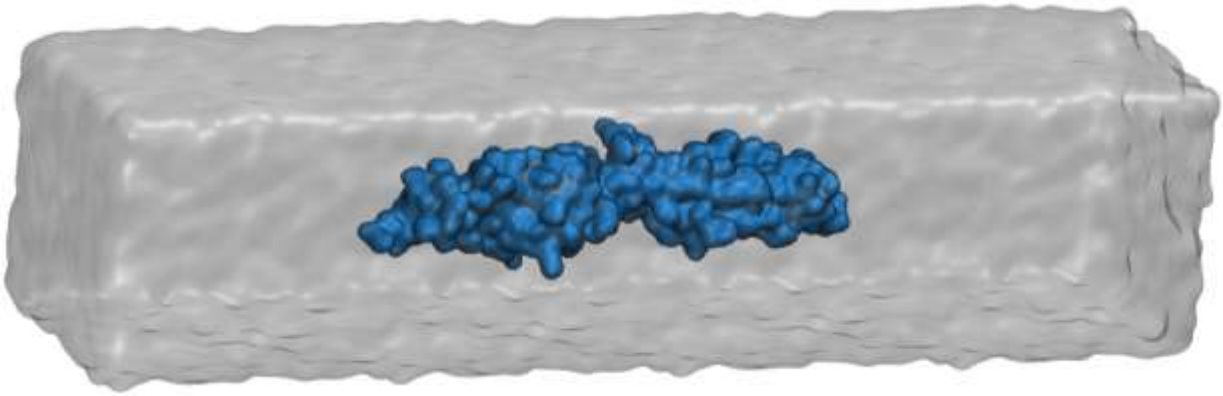

Figure 14. Cadherin-23 EC 1-2 in a 25 x 6 x 6 nm waterbox.

2. Simulation Setup: Solvated Protein Systems

The equilibrium MD simulations were performed using NAMD 2.10[41] and the Drude[9] polarizable force field. The CHARMM36 system was composed of the cadherin-23 (Chain A) segment of the PDB code 4APX structure[29] in a waterbox with 150 mM KCl. The CHARMM-GUI Drude Prepper was used to generate a series of CHARMM PSF, coordinate, and input files from an identical system amenable for equilibration with CHARMM36 non-polarizable additive force fields to a system compatible with the Drude polarizable force fields. The XPLOR-PSF, PDB, and STR files from Step 2 of the Drude Prepper were used to commence equilibration with the Drude polarizable force field. The equilibration of the system consisted of three stages outlined in Table 3.

	Stage 1	Stage 2	Stage 3
Time Step (fs)	0.1	0.1	0.5
General Langevin Damping (ps^{-1})	1.0	1.0	5
Drude Langevin Damping (ps^{-1})	20	20	20
Temperature (K)	300	300	300
Constraints	All atoms but Drude particles	Backbone	Backbone
Minimization Steps	20	20	0
Run Steps	200	10000	100000

Table 3. Configuration parameters suggested by the CHARMM-GUI Drude Prepper for equilibration of cadherin-23 EC 1 and 2 in a waterbox with 150 mM KCl.

3. Results: Drude and General Langevin Effect on Temperature Stability

In the final equilibration stage, the time step was changed to 1 fs/step and the constraints on all atoms were removed. Molecular dynamics simulations were run for 90,000 steps with a particular combination of γ_D and γ_G constants (Figure 15). Coordinates and temperature of the molecule were recorded every 0.5 ps. We observed temperature lowering with a γ_D of 5 ps^{-1} and a γ_G of 0.1 ps^{-1} and less dramatically with a γ_D of 1 ps^{-1} and a γ_G of 0.1 ps^{-1}. The most stable temperature was observed with a γ_D of 0.1 ps^{-1} and a γ_G 0.1 ps^{-1}, which should be appropriate for our SMD simulations.

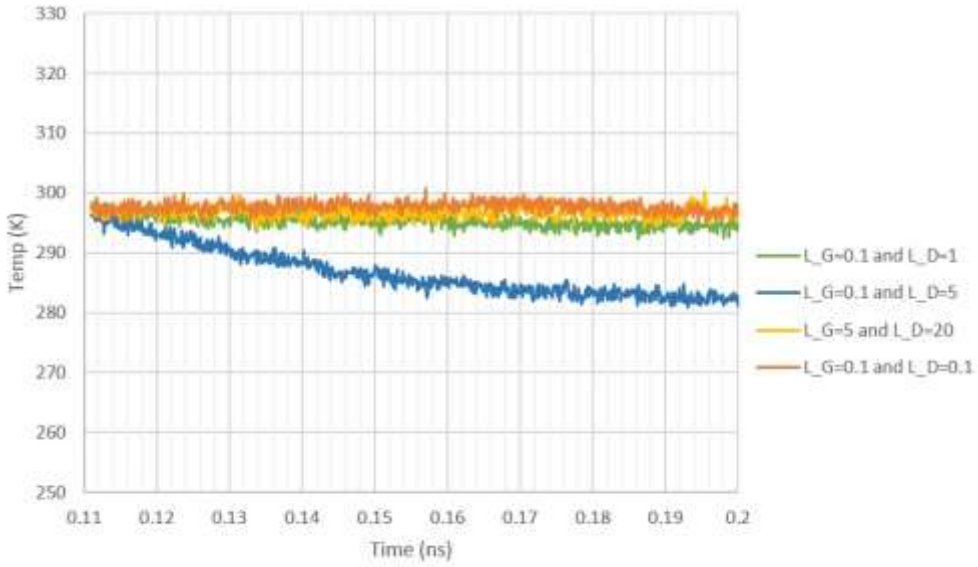

Figure 15. Temperature of the cadherin-23 EC 1 and 2 system using various Langevin value combinations.

4. Polarizable SMD Simulations of Cadherin-23 EC 1-2

Next, we seek to evaluate the ability of the selected Langevin parameters to control the temperature during SMD simulations without interfering with the dynamics of the system. The cadherin-23 EC1-2 system equilibrated with the General and Drude Langevin damping coefficients set to $\gamma_G = \gamma_D = 0.1$ was used to run an SMD simulation in which the C and N terminal C_α atoms were pulled in opposite directions (Fig 16), each with velocity 5 nm/ns.

The simulation with the aforementioned Langevin parameters was compared with a simulation in which these parameters were set to $\gamma_D = 20$ and $\gamma_G = 5$, as suggested by the CHARMM-GUI Drude Prepper. The new data shows artificially large and uncoupled N- and C-terminal forces (Fig 17), which suggests that SMD simulations carried out using the Drude polarizable force should avoid large values for γ_G and γ_D .

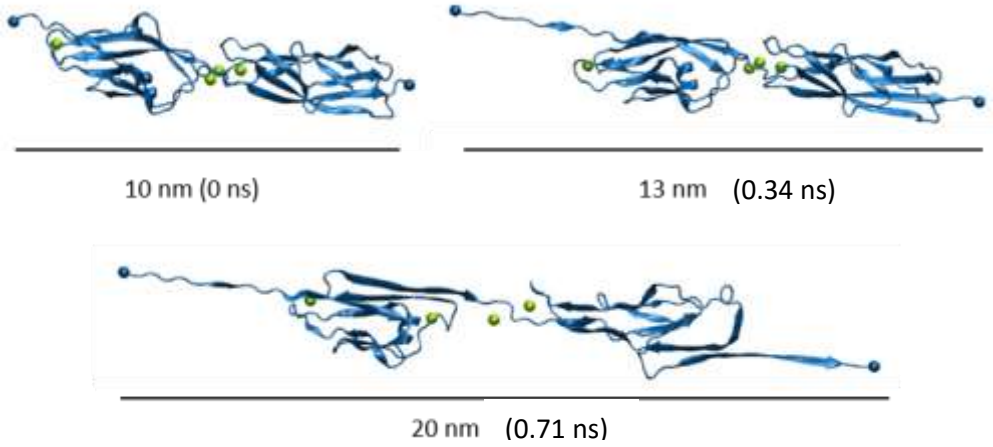

Figure 16. SMD of cadherin-23 EC 1-2 system with calcium ions in green.

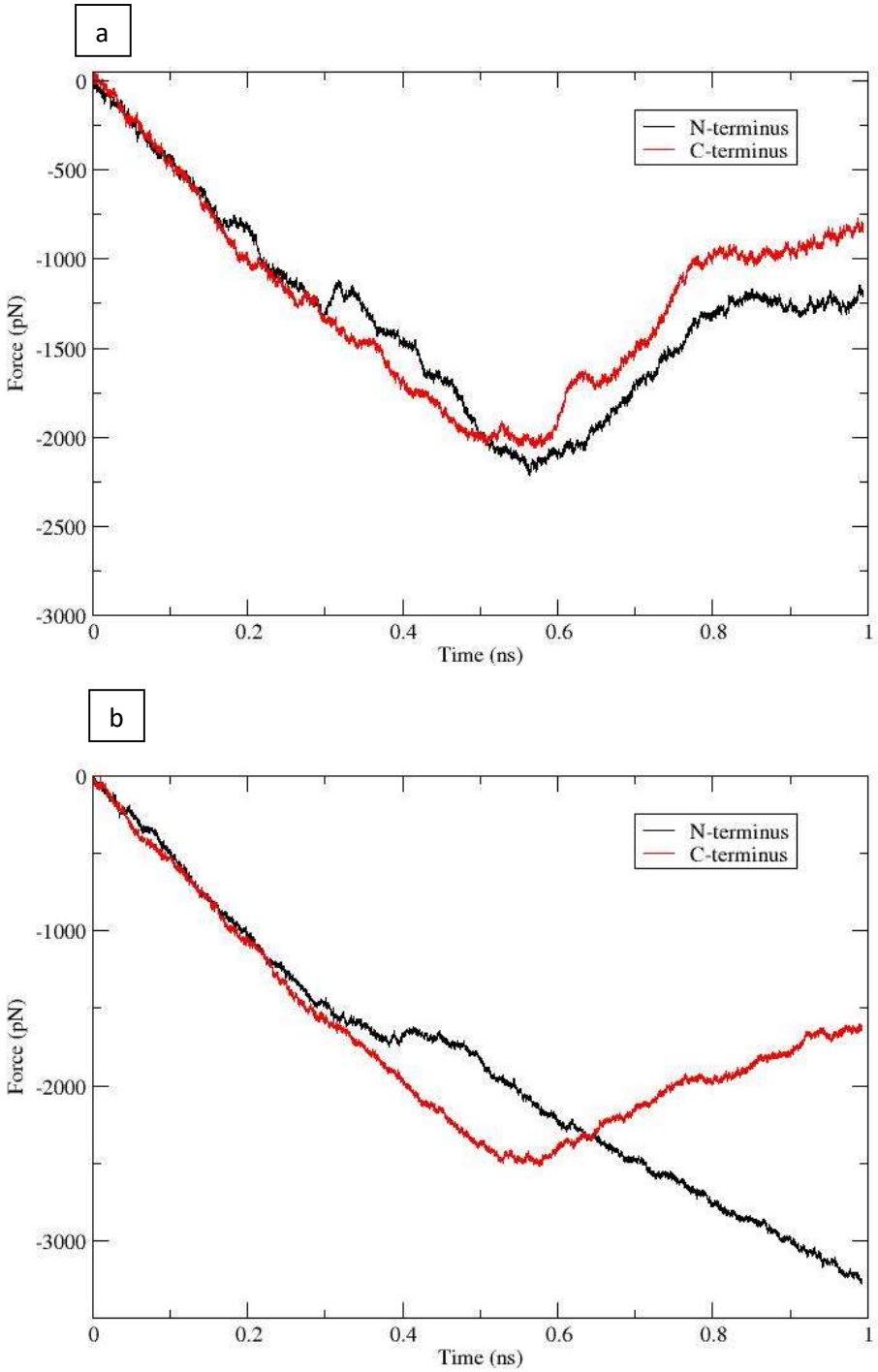

Figure 17. SMD simulations using the Drude polarizable force field. Force applied to C (black) and N terminus (red) of cadherin-23 EC 1-2 at a velocity of 10 m/s using a) γ_G = γ_D = 0.1 and b) γ_G =5 and γ_D=20.

CHAPTER 5: FUTURE OUTLOOK

There are multiple steps that could be taken in furthering this project in the short term. Thermal melting of mutants is worth analyzing for clues that can lead us to the mechanism behind certain deafness mutations. Thanks to the close relationship between structure and function, this can also be achieved by crystallizing and elucidating the structures of cadherin-23 mutant variants and comparing these to the wild-type cadherin-23 fragments.

In terms of computational studies, the aptness of the chosen Langevins could be tested using constant-force pulling on the tip-link rather than constant-velocity pulling. Because the pullings of 10 m/s are far above the speeds experienced by the tip-link in physiological conditions (the basilar membrane oscillates at velocities on the order of 0.01 m/s[43]), these simulations served as a first approximation. We plant to decrease the speeds at which the repeats are pulled in order to best represent conditions encountered by the tip-link *in vivo*. Finally, it would be interesting to observe the behavior of cadherin-23 EC 1-2 with the Drude polarizable force field and contrast it with the CHARMM36 simulations by analyzing not only the forces, but also the trajectories of the steered molecular dynamics simulations involved.

More importantly, the Drude polarizable force field coupled with steered molecular dynamics simulations can allow us to explore a host of different systems that require an ability to model divalent ions. For instance, drugs could be developed which enhance Ca^{2+}–binding ability. These drugs can be tested *in silico* with cadherin repeats, and eventually lead to minimally-invasive deafness treatments. The force field can even be used to probe Ca^{2+} signaling in the heart one day. Arrhythmias that are caused by Ca^{2+} -mishandling could be modeled using simulations, and would allow for a greater understanding of disease models. In addition, Ca^{2+} plays a large role in osteoporosis as well, and is fairly ubiquitous in salt water (~400 ppm). Thus, simulations could

pave the road to understanding disease and the environment by allowing scientists to model and observe these systems at time and length scales otherwise inaccessible.

References

1. Blackwell, D. L., Lucas, J. W. & Clarke, T. C. Summary health statistics for u.s. Adults: national health interview survey, 2012. *Vital Health Stat. 10.* 1–171 (2014). doi:24819891

2. Mitchell, R. E. & Karchmer, M. A. Chasing the Mythical Ten Percent: Parental Hearing Status of Deaf and Hard of Hearing Students in the United States. *Sign Lang. Stud.* **4,** 138–163 (2004).

3. Askew, C. *et al.* Tmc gene therapy restores auditory function in deaf mice. *Sci. Transl. Med.* **7,** 1–12 (2015).

4. El Kechai, N. *et al.* Recent advances in local drug delivery to the inner ear. *Int. J. Pharm.* **494,** 83–101 (2015).

5. Geng, R. *et al.* Noddy, a mouse harboring a missense mutation in protocadherin-15, reveals the impact of disrupting a critical interaction site between tip-link cadherins in inner ear hair cells. *J. Neurosci.* **33,** 4395–404 (2013).

6. Di Palma, F. *et al.* Mutations in Cdh23, encoding a new type of cadherin, cause stereocilia disorganization in waltzer, the mouse model for Usher syndrome type 1D. *Nat. Genet.* **27,** 103–107 (2001).

7. Siemens, J. *et al.* Cadherin 23 is a component of the tip link in hair-cell stereocilia. *Nature* **428,** 950–955 (2004).

8. Söllner, C. *et al.* Mutations in cadherin 23 affect tip links in zebrafish sensory hair cells. *Nature* **428,** 955–959 (2004).

9. Lamoureux, G. & Roux, B. Modeling induced polarization with classical Drude oscillators: Theory and molecular dynamics simulation algorithm. *J. Chem. Phys.* **119,** 3025 (2003).

10. Best, R. B. *et al.* Optimization of the Additive CHARMM All-Atom Protein Force Field Targeting Improved Sampling of the Backbone φ, ψ and Side-Chain χ 1 and χ 2 Dihedral Angles. *J. Chem. Theory Comput.* **8,** 3257–3273 (2012).

11. Reichenbach, T. & Hudspeth, a J. The physics of hearing: fluid mechanics and the active process of the inner ear. *Rep. Prog. Phys.* **77,** 076601 (2014).

12. Gillespie, P. G. & Müller, U. Mechanotransduction by hair cells: models, molecules, and mechanisms. *Cell* **139,** 33–44 (2009).

13. Pickles, J. O., Comis, S. D. & Osborne, M. P. Cross-links between stereocilia in the guinea pig organ of Corti, and their possible relation to sensory transduction. *Hear. Res.* **15,** 103–112 (1984).

14. Assad, J. a, Shepherd, G. M. & Corey, D. P. Tip-link integrity and mechanical transduction in vertebrate hair cells. *Neuron* **7,** 985–994 (1991).

15. Beurg, M., Fettiplace, R., Nam, J.-H. & Ricci, A. J. Localization of inner hair cell mechanotransducer channels using high-speed calcium imaging. *Nat. Neurosci.* **12,** 553–558 (2009).

16. Denk, W., Holt, J. R., Shepherd, G. M. G. & Corey, D. P. Calcium imaging of single stereocilia in hair cells: Localization of transduction channels at both ends of tip links. *Neuron* **15,** 1311–1321 (1995).

17. Sotomayor, M., Weihofen, W. a, Gaudet, R. & Corey, D. P. Structure of a force-conveying cadherin bond essential for inner-ear mechanotransduction. *Nature* **492,** 128–32 (2012).

18. Kazmierczak, P. *et al.* Cadherin 23 and protocadherin 15 interact to form tip-link filaments in sensory hair cells. *Nature* **449,** 87–91 (2007).

19. Kachar, Bechara, Parakkal, M, Kurc, Mauricio, Zhao, Yi-dong, Gillespie, P. High-resolution structure of hair-cell tip links. *Proc. Natl. Acad. Sci.* **97,** 13336–13341 (2000).

20. Brasch, J., Harrison, O. J., Honig, B. & Shapiro, L. Thinking outside the cell: how cadherins drive adhesion. *Trends Cell Biol.* **22,** 299–310 (2012).

21. Ogou, S. I., Yoshida Noro, C. & Takeichi, M. Calcium-dependent cell-cell adhesion molecules common to hepatocytes and teratocarcinoma stem cells. *J. Cell Biol.* **97,** 944–948 (1983).

22. Sotomayor, M., Gaudet, R. & Corey, D. P. Sorting out a promiscuous superfamily: towards cadherin connectomics. *Trends Cell Biol.* **24,** 524–536 (2014).

23. Hirano, S. & Takeichi, M. Cadherins in brain morphogenesis and wiring. *Physiol. Rev.* **92,** 597–634 (2012).

24. Astuto, L. M. *et al.* CDH23 mutation and phenotype heterogeneity: a profile of 107 diverse families with Usher syndrome and nonsyndromic deafness. *Am. J. Hum. Genet.* **71,** 262–275 (2002).

25. Bolz, H. *et al.* Mutation of CDH23, encoding a new member of the cadherin gene family, causes Usher syndrome type 1D. *Nat. Genet.* **27,** 108–112 (2001).

26. Bork, J. M. *et al.* Usher syndrome 1D and nonsyndromic autosomal recessive deafness DFNB12 are caused by allelic mutations of the novel cadherin-like gene CDH23. *Am. J. Hum. Genet.* **68,** 26–37 (2001).

27. Boëda, B. *et al.* Myosin VIIa, harmonin and cadherin 23, three Usher I gene products that cooperate to shape the sensory hair cell bundle. *EMBO J.* **21,** 6689–6699 (2002).

28. de Brouwer, A. P. M. *et al.* Mutations in the calcium-binding motifs of CDH23 and the 35delG mutation in GJB2 cause hearing loss in one family. *Hum. Genet.* **112,** 156–163 (2003).

29. Sotomayor, M., Weihofen, W. a, Gaudet, R. & Corey, D. P. Structural determinants of cadherin-23 function in hearing and deafness. *Neuron* **66,** 85–100 (2010).

30. Bosher, S. K. & Warren, R. L. Very low calcium content of cochlear endolymph, an extracellular fluid. *Nature* **273,** 377–378 (1978).

31. Hara, A., Salt, A. N. & Thalmann, R. Perilymph composition in scala tympani of the cochlea: influence of cerebrospinal fluid. *Hear. Res.* **42,** 265–271 (1989).

32. Li, H. *et al.* Representation of Ion–Protein Interactions Using the Drude Polarizable Force-Field. *J. Phys. Chem. B* 150204133028006 (2015). doi:10.1021/jp510560k

33. Howard, J. & Hudspeth, a J. Compliance of the hair bundle associated with gating of mechanoelectrical transduction channels in the bullfrog's saccular hair cell. *Neuron* **1,** 189–199 (1988).

34. Dechavanne, V. *et al.* A high-throughput protein refolding screen in 96-well format combined

with design of experiments to optimize the refolding conditions. *Protein Expr. Purif.* **75,** 192–203 (2011).

35. Wagatsuma, M. *et al.* Distribution and frequencies of CDH23 mutations in Japanese patients with non-syndromic hearing loss. *Clin. Genet.* **72,** 339–344 (2007).

36. Ericsson, U. B., Hallberg, B. M., DeTitta, G. T., Dekker, N. & Nordlund, P. Thermofluor-based high-throughput stability optimization of proteins for structural studies. *Anal. Biochem.* **357,** 289–298 (2006).

37. Cheung, E. L. M. & Corey, D. P. Ca2+ Changes the Force Sensitivity of the Hair-Cell Transduction Channel. *Biophys. J.* **90,** 124–139 (2006).

38. Dehez, F., Tarek, M. & Chipot, C. Energetics of ion transport in a peptide nanotube. *J. Phys. Chem. B* **111,** 10633–10635 (2007).

39. Lamoureux, G. & Roux, B. Absolute hydration free energy scale for alkali and halide ions established from simulations with a polarizable force field. *J. Phys. Chem. B* **110,** 3308–22 (2006).

40. Kalé, L. *et al.* NAMD2: Greater Scalability for Parallel Molecular Dynamics. *J. Comput. Phys.* **151,** 283–312 (1999).

41. Phillips, J. C. *et al.* Scalable molecular dynamics with NAMD. *J. Comput. Chem.* **26,** 1781–1802 (2005).

42. Jo, S., Kim, T., Iyer, V. G. & Im, W. CHARMM-GUI: A Web-Based Graphical User Interface for CHARMM. *J. Comput. Chem.* **29,** 1859–1865 (2008).

43. Ruggero, M. A., Rich, N. C., Recio, A., Narayan, S. S. & Robles, L. Basilar-membrane responses to tones at the base of the chinchilla cochlea. *J. Acoust. Soc. Am.* **101,** 2151–63 (1997).

44. Dror, A. a & Avraham, K. B. Hearing loss: mechanisms revealed by genetics and cell biology. *Annu. Rev. Genet.* **43,** 411–37 (2009).

45. Ashmore, J. Cochlear Outer Hair Cell Motility. *Physiol. Rev.* **88,** 173–210 (2008).

46. Furness, D. N., Mahendrasingam, S., Ohashi, M., Fettiplace, R. & Hackney, C. M. The dimensions and composition of stereociliary rootlets in mammalian cochlear hair cells: comparison between high- and low-frequency cells and evidence for a connection to the lateral membrane. *J. Neurosci.* **28,** 6342–53 (2008).

47. GE Healthcare. Size exclusion chromatography: Principles and Methods. *GE Heal. Handbooks* 139 (2012).

48. Illingworth, C. J. & Domene, C. Many-body effects and simulations of potassium channels. *Proc. R. Soc. A Math. Phys. Eng. Sci.* **465,** 1701–1716 (2009).